Chapter 6

Relaxor-Super-Paraelectric Behavior and Crystal

Field Driven Spin-Phonon Coupling in Pyrochlore

$Eu_2Ti_2O_7$

6.1 Introduction

The search for new type-II multiferroic materials has become the current interest globally to pursuit the benefits of the intrinsic mutual control between ferroelectric (FE) and the magnetic orders which may produce materials with better performance [266–268]. In this regard pyrochlore materials are very promising. The pyrochlores are geometrically frustrated and the inherent spin frustration leads to different low temperature exotic states by means of proper balance among the different competing exchange interactions, dipolar interactions and crystal field effect [1,80,81,269–272]. Moreover, the discovery of the ferroelectricity in spin ice $Dy_2Ti_2O_7$ and $Ho_2Ti_2O_7$ compounds provided a new impetus towards the search for ferroelectricity in pyrochlore materials [273,274]. Interestingly, multiple ferroelectric transitions with different origins were observed in the dielectric property of these compounds [273]. Two successive ferroelectric transitions were observed at 25 K and 13 K in the polycrystalline $Dy_2Ti_2O_7$ system [275] On the other hand, similar transitions were observed in the isostructural $Ho_2Ti_2O_7$ at 60 K and 23 K [274]. It was inferred that the higher temperature transitions (i.e., at 25 K for $Dy_2Ti_2O_7$ and 60 K for $Ho_2Ti_2O_7$) are related to the structural origin [276]. The lower temperature transitions (23 K for $Ho_2Ti_2O_7$ and 13 K for $Dy_2Ti_2O_7$) are essentially emerged from the nucleation of the electric dipoles driven by the non-collinear spin ordering [273,275]. Again, a low temperature ferroelectric transition at 1.2 K was observed in the single crystal of $Dy_2Ti_2O_7$ which is possibly associated to the emergence of a spin-ice state [273].

In previous study on the isostructural pyrochlore titanate $Eu_2Ti_2O_7$, a plateau region below 150 K which is triggered by the crystal field effect was observed [12]. Further, X-ray absorption spectroscopy (XAS) measurements showed that the Ti ions occupy a distorted

octahedral site (O_h) owing to the presence of an interstitial anionic site (8a) adjacent to the TiO_6 octahedra [277]. It is expected that such octahedral distortion may lead to the generation of electric dipoles and thus the ferroelectricity. The dielectric study of $Eu_2Ti_2O_7$ has not yet been reported. Thus, here we spot light mainly on dielectric and Raman spectroscopy studies on $Eu_2Ti_2O_7$ pyrochlore. The main focus of this report remains in the existence of appreciable value of dielectric constant with low tangent loss, a clear dielectric anomaly in the form of a broad peak below 150 K, observation of super-paraelectricity, anomalous softening of few (at least two) Raman modes near the temperature of dielectric anomaly along with the appearance of an additional peak on lowering the temperature indicating a local symmetry breaking. Additionally, a dielectric transition below 40 K, related to strong spin freezing has been described.

6.2 Experimental

The polycrystalline pyrochlore $Eu_2Ti_2O_7$ (ETO) were prepared via solid state reaction route as described elsewhere [12]. The mixture of starting materials (with a high purity of greater than 99.99%) Eu_2O_3, and TiO_2 were taken in appropriate proportion and was ground for around 30 minutes and then heated at 1000^0 C in air for 24 hours. After cooling to room temperature, it was again ground for 20 minutes and heated at 1100^0 C for 36 hours. This process of heat treatment was repeated further at 1200^0 C and 1250^0 C. The final powder was reground and pressed into pellets with a diameter of around 10 mm and width around 1 to 2 mm. These pellets were sintered at 1300^0 C for 48 hours. Finally, it was cooled to room temperature with a very slow rate (0.5^0 C/minute) to avoid cracks in pellets. A piece of the sintered pellet was ground for XRD and Raman measurements. The XRD measurements of powdered sample was carried out using a Rigaku Miniflex-II powder diffractometer. The XRD

pattern was analyzed with a Fullprof software using Rietveld method. Raman spectra of the powdered sample were taken using a Renishaw inVia Raman spectrometer with 532 nm line of a diode pumped solid state laser generating power of 5 mW mm^{-2}. The sample was put in a quartz sample holder inside a cooling/heating sample cell (THMS-600) that is connected to a temperature controller (TMS94) to control the temperature of the sample under study. The incident laser beam was focused on the sample through the transparent window of the THMS-600 by a 50× short distance objective attached to the Leica DM 2500M microscope. Backscattering geometry was used to collect the scattered beam through the same objective, and a 2400 grooves/mm grating was used as the dispersion element. The spectra were recorded with a spectral resolution of ~1 cm^{-1}. Dielectric measurements were carried out using a highly sensitive Keysight E4980A Precision LCR meter with a He-cooled closed cycle refrigerator (CCR).

6.3 Results and discussions

6.3.1 Structural analysis

The XRD patterns along with the Rietveld refinements of ETO at room temperature is shown in Fig 6.1, which is reported in earlier study [12,277]. The analysis of refined data showed that the system crystallized in single phase cubic structure having Fd$\bar{3}$m symmetry. Further analysis shows that there are strong octahedral distortion as the bond angles of O(1)-Ti-O(1) are estimated to be 94.514^0 and 85.486^0 which are near to the reported value of bond angles in a similar system with octahedral distortion associated to TiO$_6$ [278]. The large difference between the ionic radii of Ti^{4+} and Eu^{3+} ions and the existence of 8a-site oxygen vacancy adjacent to the TiO$_6$ octahedra on the ab-plane are supposed to be key reason of distortion in TiO$_6$ octahedra [279].
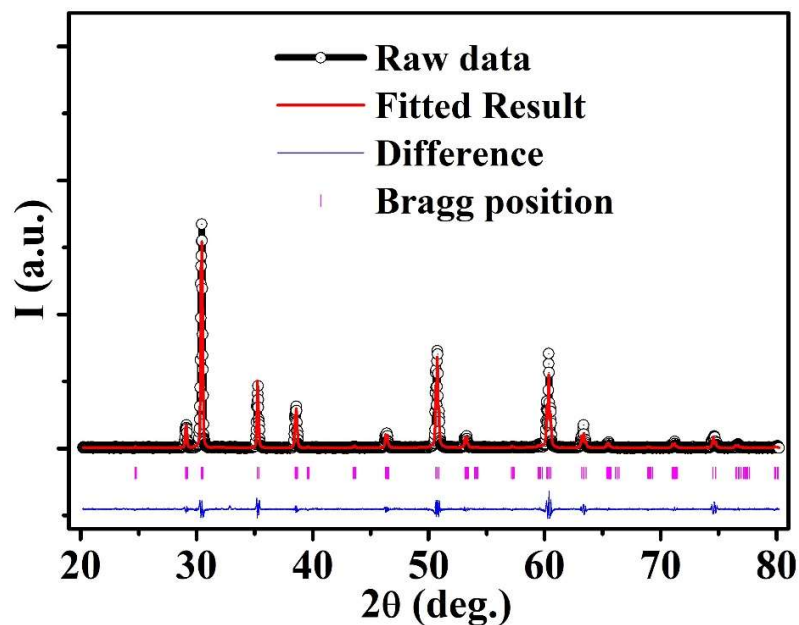
Figure 6.1: *X-ray diffraction pattern with Rietveld refinement with space group Fd-3m of Eu$_2$Ti$_2$O$_7$ collected at room temperature (300 K).*

6.3.2 Raman study

Raman spectroscopy is a powerful tool which provides precise information about the local lattice dynamics/disorder of the micro and macro-phases in the system. It is a surface sensitive technique as the used excitation energy (near IR region) is relatively less penetrating. The ideal simple/face-centered cubic system (space group Pm-3m or Fm-3m) possesses the center of symmetry, thus does not allow Raman active modes. However, a few active Raman modes may appear due to the exchanges of elements of different site having different radii which may disrupt the crystal symmetry. The number of bands and relative intensity observed in Raman spectra measures the degree of structural deviation from the ideal cubic symmetry.

It was extensively showed by group theory calculations on pyrochlore lattice A$_2$B$_2$O$_7$ (Oxygen has two sites O1/48f and O2/8b) having the symmetry Fd-3m that it should show six Raman active fundamental modes which are demonstrated by the A$_{1g}$+E$_g$+4F$_{2g}$ irreducible

representations [278,279]. Only the motions of oxygen atoms are involved for these modes. The five modes $A_{1g}+E_g+3F_{2g}$ arise due to the vibrations of the oxygen atoms (O1) situated at 48f site and bonded to two A and two B cations while only a single F_{2g} mode originates from the motions of oxygens (O2) located at 8b which are tetrahedrally attached to the A cations. However, the calculation also showed that there should be total 26 zone center modes which is given by; $\Gamma = A_{1g}+E_g+2F_{1g}+4F_{2g}+ 3A_{2u}+3E_u+8F_{1u}+4F_{2u}$. Here, $8F_{1u}$ are infrared active whereas $2F_{1g}$, $3A_{2u}$, $3E_u$, $4F_{2u}$ are optically inactive [279].

We have taken the Raman spectra of ETO at different temperatures. Fig. 6.2 represents the Raman spectra of ETO only at three different temperatures to avoid complexity. It has been inferred that the detected peaks in the spectra are in accordance with pyrochlore-like phase and the symmetry species of the observed bands has been tentatively assigned according to the previously reported Raman spectra of the pyrochlores [14,123,280–282]. The weak peak ω_1 at low wave-number side (190-207 cm^{-1}) has been assigned to F_{2g} mode. On the basis of previous literature on similar pyrochlore materials, the most intense band at 306 cm^{-1} and a very weak shoulder at 321 cm^{-1} (which is only visible on taking a closer look as shown in the inset of Fig. 5.2) can be unambiguously attributed to F_{2g} and E_g modes. Thus, the strongest band of ETO centred around ω_2 (~306-307 cm^{-1}) is the combination of two modes (F_{2g} and E_g) with comparable wave-numbers and arises due to O-Eu-O bending vibrations [14,280]. The weaker band around ω_3 (~426-431 cm^{-1}) are characteristics of the Ti-O vibrations and is assigned to F_{2g} mode. This mode is very sensitive to the cation attached with the $Ti_2O_7^{-6}$ anion [283]. Another strong peak ω_4 (~512-516 cm^{-1}) is attributed to Eu-O stretching vibrations and has been assigned as A_{1g} mode of phonon. Another low intensity band observed around 580 cm^{-1} (ω_5) can be attributed to F_{2g} mode. The broad band appeared at higher frequency side around

ω_6 (~692 cm^{-1}) has been assigned to a combined mode from the F_{2g} band (190-207 cm^{-1}) and A_{1g} band (512-515 cm^{-1}) similar to other pyrochlores [284]. Most interestingly, on lowering the temperature below 200 K, this band (~ω_6) starts decoupling and shows the emergence of an additional band immediately below the ω_6 (~692 cm^{-1}) band at around 660-680 cm^{-1} (shown in the right panel of the Fig. 6.3). This additional Raman active mode band suggests a local symmetry breaking which might be due to the presence of strong dielectric dispersion below 200 K (discussed later in this report). The Raman modes appearing above 600 cm^{-1} for the pyrochlore titanates are mainly originated from the Ti-O stretching vibrations [285].
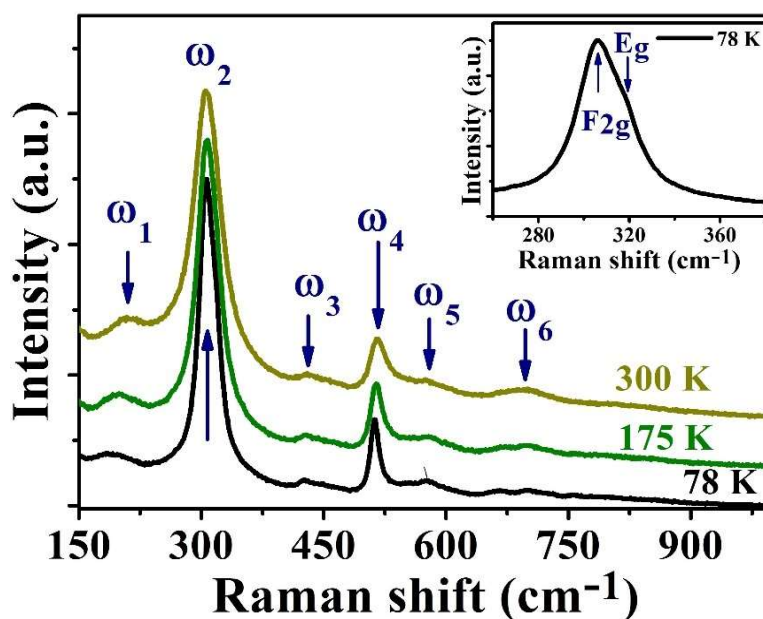

Figure 6.2: *Raman spectra at 78 K, 175 K and 300 K respectively. The inset shows the decoupling of F_{2g} and E_g modes at 78 K.*

The variation of the Raman excitation frequency (ω) as a function of temperature for the two most intense modes (ω_2, ω_4) are shown in Fig. 6.4(a). In general, according to Balkanski, in the absence of any external perturbation like spin-phonon coupling, electron-

phonon coupling, magnetostriction, structural transition etc., the temperature variation of Raman modes should follow the anharmonic equation as given by [178,211],

$$\omega_{anh}(T) = \omega_0 - C \left[1 + 2/\{exp(\hbar\omega_0/k_BT) - 1\}\right] \qquad (6.1)$$

where ω_0 and C are the adjustable parameters, T is the temperature, $\hbar$ is reduced Planck's constant and k_B is the Boltzmann's constant. This expression suggests that the Raman peak should shift towards higher wave-number side (i.e., hardening of bonds) and pursue a plateau on decreasing temperature. However, if there exists any of the aforementioned perturbations, the Raman modes show anomalous softening from a critical temperature as they deviate from the anharmonic equation [211].
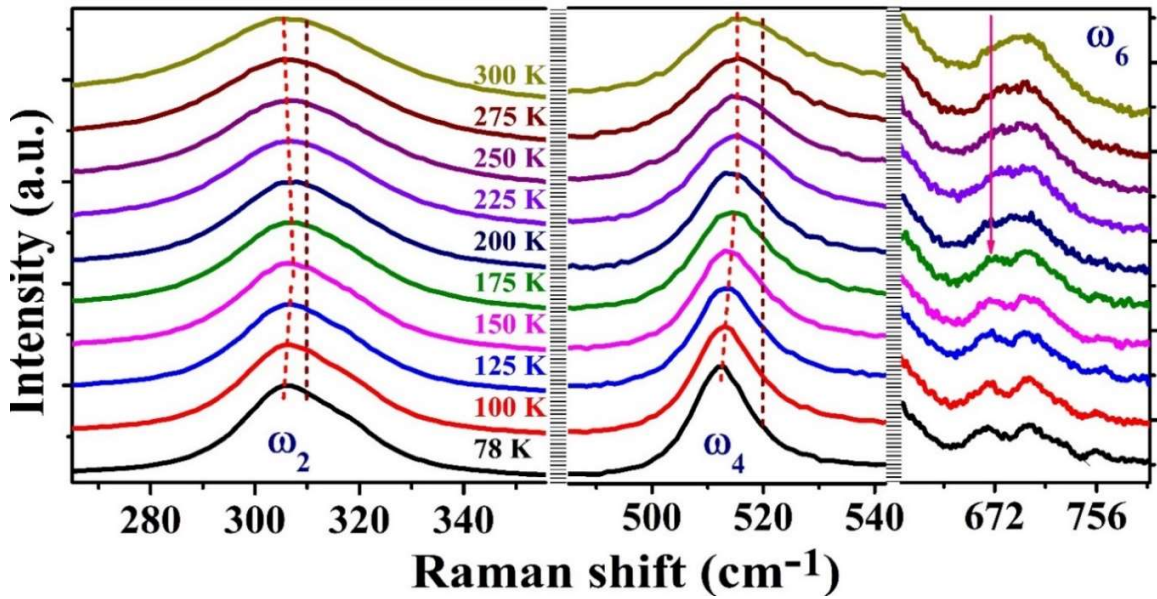

Figure 6.3: *Raman spectrum at different temperatures for the bands centered around ω_2 (left panel), ω_4 (middle panel) and ω_6 (right panel).*

It is very surprising to observe that for both the Raman modes (ω_2, ω_4), the excitation frequencies showed prominent anomalous softening near 150 K (Fig. 6.3 & 6.4a) and line

width variation with the temperature which also showed an anomalous behavior across 150 K (Fig. 6.4(b)), thus indicating towards the presence of some other contributing factors other than the simple anharmonicity. It is important to mention here that for ETO, the magnetization curve showed short-range magnetic ordering below 150 K, attributed to crystal field (CF) effect [12]. Hence, it may be plausible to state that the underlying CF effect may be a contributing factor to the modulation of the phonon frequencies, causing a deviation from the anharmonic equation. The ETO is highly insulating in nature, thus there is no possibility of the presence of electron-phonon coupling. However, the spin-orbit interaction within Eu^{3+} ions lead its electronic pattern consisting of ground state $^7F_0$ (non-magnetic) along with the first excited $^7F_1$ (which is basically magnetic) lying closely above it. The CF-level again splits into further levels e.g., $^7F_1$ splits into a singlet and a doublet. Thus, Eu^{3+} has appreciable magnetic susceptibility rather than having a non-magnetic ground state, which is already introduced in
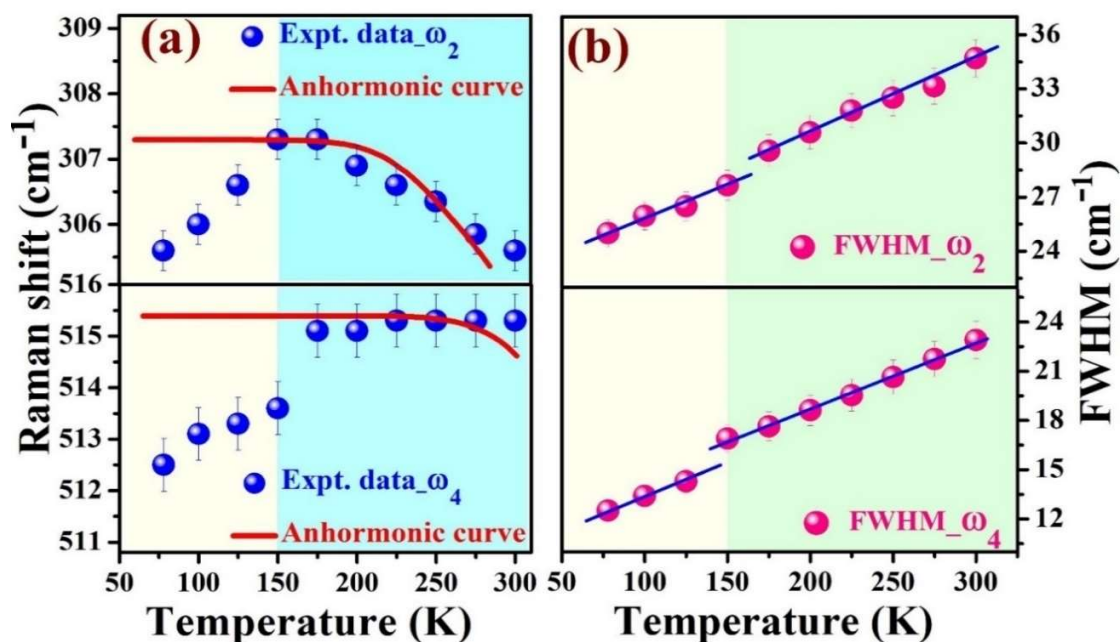

Figure 6.4: *The temperature variation of (a) phonon frequency and (b) FWHM for the two intense modes ω_2 and ω_4.*

ref. 15. Thus, short-range magnetic ordering below 150 K (see the difference between FC and ZFC magnetization below this temperature) has been detected in and hence observed phonon softening might be due to spin-phonon coupling. Examples of such phonon anomalies due to the spin-phonon coupling can be found in earlier report by [286].

5.3.3 Dielectric study

As discussed, in ETO, the XAS study revealed the existence of strong octahedral distortion in the TiO_6 octahedra due to the presence of interstitial site 8a [277]. The Raman study also showed a local symmetry breaking in ETO below 200 K which is related to the TiO_6 octahedra. Such octahedral distortion of TiO_6 in similar pyrochlore $Ho_2Ti_2O_7$ was considered to be the key factor for producing the net electrical polarization leading to the ferroelectricity [274]. Thus, we have measured relative permittivity of ETO elaborately.
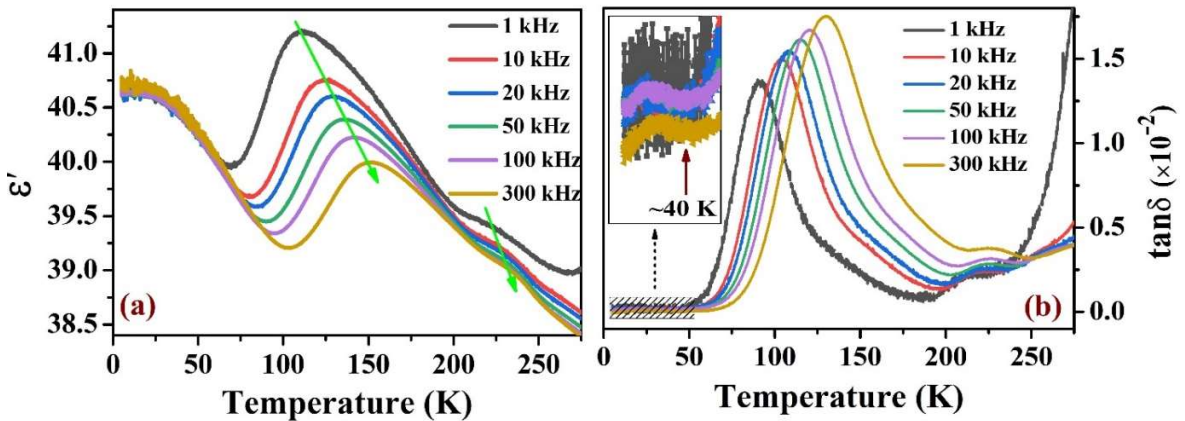

Figure 6.5: *The thermal variation of (a) relative permittivity of ETO and (b) tangent loss at different frequencies.*

Fig. 6.5(a) demonstrates the variation of relative permittivity (ε') vs. Temperature (T) curves of ETO measured at different frequencies while the corresponding loss ($\tan\delta$) factor is shown in Fig 6.5(b). The relative permittivity increases on decreasing temperature and shows a strong diffuse dielectric relaxation peak with maximum permittivity (ε'_m) at a temperature T_m (~135 K at 50 kHz). Similar relaxation peaks have been observed in dielectric loss spectrum as well. This shows that a transition occurs below 200 K for ETO. Interestingly, the anomalous softening of the phonon modes and the slope change of magnetization due to the CF effect also commence below 200 K. This is an indication that the CF, phonons and electrical dipoles are
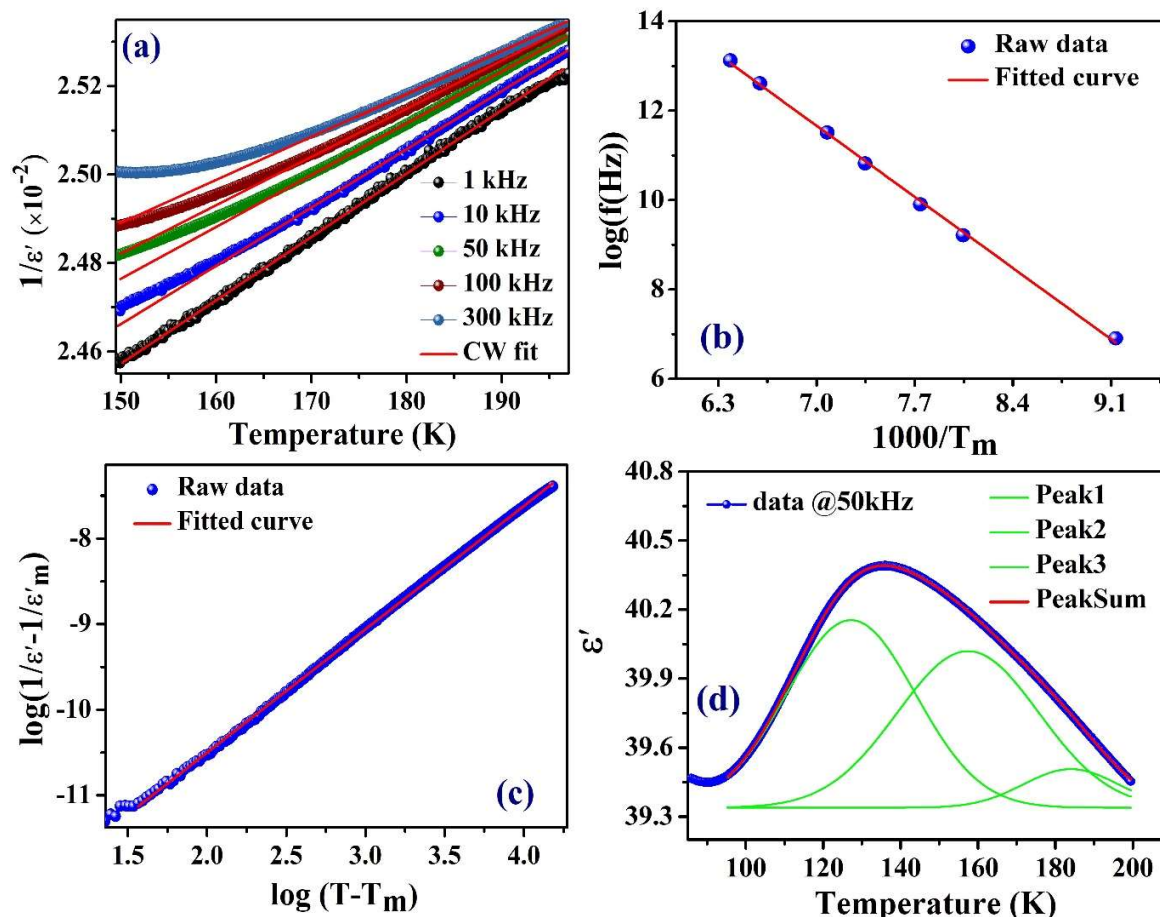

Figure 6.6: _(a) CW fitting at different frequency. (b) The Arrhenius fitting for relaxation peak. (c) The modified CW fitting and (d) showing asymmetric nature of the relative permittivity of ETO around T_m at a frequency of 50 kHz._

mutually entangled with each other. Such coupling in this ETO system is very interesting and remained hitherto unreported. As the frequency (*f*) increases, the relaxation peaks grow to be broader, the $T_m(f)$ shifts towards higher temperature. Additionally, two weak relaxation peaks, one above 200 K and second below 40 K (which is seen only in tanδ curves, inset of Fig. 6.5b) in ETO has been observed. It can be unambiguously plausible to elucidate the underlying origin of the observed dielectric transition in ETO at lower temperature might be related to the emergence of strong spin-spin correlation which commences below the onset of spin freezing ~40 K as there is strong spin freezing below 40 K [12]. However, other dielectric transitions observed in ETO can be related to local symmetry breaking/decoupling of Raman mode below 200 K, as there is no strong spin-spin correlation present above 40 K. Further, detailed analysis of dielectric relaxation of strong peak (in the range 70 K-200 K) has been carried out as discussed below.

In the paraelectric region, ε'-T curves can be fitted with the Curie-Weiss (CW) law; $\varepsilon' = C/(T - T_{CW})$ [287]. Data was well fitted at low frequency (@1kHz), which could be seen in the Fig 6.6(a). The CW fitting at 1 kHz gives the value of Curie constant (C) of the order of ~10^5, which is generally observed for displacive ferroelectrics and supports existence of relaxor state [287]. However, at higher frequencies, the variation of ε' start to diverge from the CW law due to increase of transition temperature (T_m), where fitting range is not far away from the T_m. It has been observed that the CW curve that shows slightly different slopes (Fig. 6.6(a)) at different applied frequencies indicates the short-range ordering among induced electrical dipoles, while for an ideal ferroelectric they should be frequency independent. Also, the deviation of ε' from the CW law, above T_m, within a specific temperature range is the features of one of the relaxor states [288].

The feasible explanation of dispersion in both $\varepsilon'_m(f)$ and tanδ ETO is the formation of many small Polar Nano Regions (PNRs) and these PNRs responses differently for different frequency. It could be interpreted as dipolar glass which is analogous to the conventional spin glass model in magnetism, where dipoles are frozen at lower temperature. In this framework, the "frequency (f) vs. temperature (T_m)" curves follows Vogel-Fulcher (VF) law [289,290], given by $f = f_0 exp\left[-T_a/(T_m - T_{vf})\right]$. Where, T_{vf} (VF freezing temperature) is the temperature at which the dynamics of dipolar cluster polarization is no longer thermally activated and only entity that survives is their boundary motions and $T_a = E_a/K_B$, where E_a corresponds to the activation energy and K_B is the Boltzmann constant. If inter-dipolar-interaction is weak then dipoles do not freeze cooperatively and may vibrate through external ac electric field at finite temperature, for this case f vs. T_m follows thermally activated Arrhenius relation ($T_{vf} \rightarrow 0$ K) [288], $f = f_0 exp(-T_a/T_m)$. For ETO the data was best fitted using Arrhenius equation (Fig. 6.6b) with $E_a \sim 0.19$ eV. Slight high value of activation energy might be attributed to the weak coupling between dipolar clusters and it is the order (~0.1 eV) of activation energy of a typical relaxor-ferroelectric [288,291]. The calculated value of relaxation frequency, f_0 is of the order of few THz (10^{12} Hz).

Furthermore, the existence of local pseudo-cubic symmetry was observed to be responsible for the relaxor behavior with diffuse type of phase transition [292,293]. The degree of diffuseness in dielectric was calculated by fitting the data using modified Curie-Weiss (CW) law [294], which is given by

$$\frac{1}{\varepsilon} - \frac{1}{\varepsilon_m} = \left(\frac{T-T_m}{\Delta}\right)^{\gamma} \tag{6.2}$$

The calculated critical parameter γ, a determining factor of the degree of diffuseness, was found to be ~1.5, thus suggesting ferroelectric-relaxor state in ETO (as $\gamma = 1$ suggests for normal ferroelectric and $\gamma = 2$ suggests for ideal relaxor ferroelectric). Similar ferroelectric relaxor state was also observed in pyrochlore $Ho_2Ti_2O_7$ and $Dy_2Ti_2O_7$ as introduced earlier. It can be noted that the permittivity decreases on further lowering the temperature showing a minimum (around 90 K at 50 kHz) and again starts increasing on further cooling. This behavior is probably due to the electronic contribution at the interface of sample and electrode similar to Tb_2CoMnO_6 film [288].

Another interesting behavior that was also observed in dielectric relaxor peak, is the asymmetrical diffused phase transition around T_m. Mathematical assumption suggests that the size distribution of PNRs should follow Gaussian profile and hence ε' will be symmetric around T_m [295]. In contrast, for ETO, in the temperature ranges $T < T_m$ and $T > T_m$, we notice that the ε' varies with different rates and it can be fitted with superposition of multiple Gaussian distribution around T_m (Fig. 6.6d). Thus, physically it indicates multiple PNRs are participating in dielectric relaxation with significant size distribution, whose microscopic origin might be different and may induce random fields within system. At lower temperature, above mentioned PNRs start interacting and due to dissimilar sizes, they respond in different manners with temperature variation as well as with varying external frequency. This feature is signature behavior of super-paraelectric state of a system [288,295]. The super-paraelectric model demonstrate the existence of local symmetry breaking within a higher global symmetric matrix [295]. Thus, emergence of a super-paraelectric state have been inferred for ETO instead of dipolar glass.

6.4 Conclusion

The structural and electrical properties of the pyrochlore oxide $Eu_2Ti_2O_7$ have been investigated. The temperature dependent Raman spectroscopy study of ETO revealed a local symmetry breaking 200 K which is attributed to the TiO_6 octahedra. It also probed the existence of possible crystal field driven spin-phonon coupling in the system as the Raman modes showed prominent anomalous softening below ~150 K. The thermal variation of dielectric constant of ETO showed a glassy diffused dielectric relaxor transition around150 K, implying that the crystal field, phonon and electric dipoles are correlated to each other in this system. Furthermore, analysis of dielectric relaxation shows existence of super-paraelectric state has been inferred in the system rather than dipolar glass. Most importantly, a dielectric transition at lower temperature (below 40 K) were observed, which is related to spin-spin correlation.